# The MICE Ionisation Cooling Demonstration: Technical Note

V. Blackmore, C. Hunt, J-B. Lagrange, J. Pasternak, C. Rogers, P. Snopok, H. Witte
on the behalf of the MICE Collaboration

Removal of the RFCC module from the MICE programme necessitated a lattice redesign such that sustainable muon ionisation cooling could be demonstrated by 2017. Two lattice designs are presented, a reference and alternative design, that use existing components. The performance in 4D is compared, while 6D performance is under study. The reference lattice is selected as the future MICE cooling cell for the demonstration of ionisation cooling.

## 1 Ionisation Cooling

Muons are produced occupying a large area of phase space (*i.e.* large emittance), which must be condensed before acceleration. Muon beams are produced at the front end of a Neutrino Factory (NF) [1] with an emittance of 15–20 $\pi$ mm.rad, which must be reduced to 2–5 $\pi$ mm.rad. A Muon Collider [2] requires further cooling, reducing the emittance to 0.4 $\pi$ mm.rad in the transverse plane, and 1 $\pi$ mm.rad in the longitudinal plane. Synchrotron radiation and stochastic cooling techniques are unsuitable for muon beams due to the short muon lifetime.

Ionisation cooling is the only process that can efficiently reduce the emittance of a muon beam within its lifetime. A beam is passed through a low-$Z$ material ("absorber"), losing energy by ionisation, reducing the phase-space area it occupies. This is sustainable if the beam is re-accelerated, restoring energy the energy lost in the absorbers. The rate of change of transverse (2D) normalised emittance, $\varepsilon_N$, is given by,

$$\frac{d\varepsilon_N}{ds} \simeq \frac{\varepsilon_N}{\beta^2 E_\mu}\left\langle\frac{dE}{ds}\right\rangle + \frac{\beta_\perp (13.6\,\mathrm{MeV})^2}{2\beta^3 E_\mu m_\mu X_0}\,, \tag{1}$$

where $\beta = \frac{p}{E}$ is the relativistic velocity, $E_\mu$ the energy, $\frac{dE}{ds}$ the energy lost by ionization, $m_\mu$ the mass of the muon, $X_0$ the radiation length of the absorber and $\beta_\perp$ the transverse beta function at the absorber. The first term of this equation describes "cooling" by ionisation energy loss, and the second term describes "heating" by multiple Coulomb scattering. When these terms are equal, the equilibrium emittance is given by,

$$\varepsilon_{\mathrm{eq}} \simeq \frac{\beta_\perp (13.6\,\mathrm{MeV})^2}{2\beta m_\mu X_0}\left\langle\frac{dE}{ds}\right\rangle^{-1}. \tag{2}$$

The smaller the equilibrium emittance, the more efficient the emittance reduction. Hence, a cooling channel will minimise $\beta_\perp$ at the absorber and maximise $X_0\langle\frac{dE}{ds}\rangle$. $\beta_\perp$ is most effectively minimised by using a solenoidal focussing channel, and $X_0\langle\frac{dE}{ds}\rangle$ is maximised by using a low-$Z$ absorber such as liquid hydrogen ($LH_2$) or lithium hydride (LiH).

## 2 The Muon Ionisation Cooling Experiment

The Muon Ionisation Cooling Experiment (MICE) was designed to measure the ionisation cooling efficiency of a section of a "Super Focus-Focus" (SFOFO) lattice cell [3] based on the Neutrino Factory Feasibility Study 2 design [4]. As ionisation cooling depends on momentum (Equation 1), the cell performance will be measured over a range of momenta, and momentum spreads, from 140–240 MeV/$c$.

Table 1: The 'as built' dimensions of the MICE coils, as also shown in Figure 1.

| Module | Coil | Length (mm) | Inner Radius (mm) | Outer Radius (mm) | $N_{\mathrm{turns}}$ | $N_{\mathrm{layers}}$ |
|---|---|---|---|---|---|---|
| SS | M1 (Match 1) | 201.3 | 258.0 | 304.2 | 115 | 42 |
| SS | M2 (Match 2) | 199.5 | 258.0 | 288.9 | 114 | 28 |
| SS | E1 (End 1) | 110.6 | 258.0 | 318.9 | 64 | 56 |
| SS | C (Centre) | 1314.3 | 258.0 | 280.1 | 768 | 20 |
| SS | E2 (End 2) | 110.6 | 258.0 | 325.8 | 64 | 62 |
| AFC | FC (Focus) | 213.3 | 267.0 | 361.8 | 134 | 84 |

The expected reduction in emittance across a single absorber is small. Hence MICE measures $(x, y, z, p_x, p_y, p_z, t)$ for individual muons before and after the cooling channel using scintillating fibre (SciFi) tracker planes and time-of-flight (TOF) counters. Transverse emittance is measured to $\pm 0.01\,\pi$ mm.rad and particle ID detectors ensure the purity of the muon beam. The MICE Muon Beam and detector systems are documented in [5], and its characterised beams in [6].

MICE at Step V was designed to consist of three classes of superconducing solenoid modules: Spectrometer Solenoids (SS), Absorber Focus Coils (AFC), and a RFCC (RF cavities and Coupling Coil). The built dimensions of the SS and AFC magnets are given in Table 1 and are layed out in Figure 1.

The SS (Figure 1a) modules consist of five superconducting coils wound on a common bobbin. Three coils (E1, E2, C) operate in series to produce the uniform 4 T field region where a scintillating fibre tracker is located. The remaining coils (M1 and M2) match the beam to/from the cooling channel. One SS is situated upstream of the cooling channel (SSU) and another downstream (SSD). The upstream Spectrometer Solenoid also contains a variable amount of high-$Z$ material upstream of the tracker, known as the "Diffuser", which is used to vary the initial beam emittance before the cooling channel. Both SSU and SSD have been field mapped and perform to specification.

The AFC (Figure 1b) modules consist of two identical coils, wound on a common bobbin, bracketing a low-$Z$ absorber (in the Step IV configuration). Table 2 lists the properties of low-$Z$ absorbers that can be used in MICE. This magnet provides a range of $\beta_\perp$ at the centre of the absorber, reducing the influence of the multiple scattering term in Equation 1. The coils in the AFC can be powered in either the same ("Solenoid Mode") or opposite sense ("Flip Mode"). When powered in Flip Mode, the sign of the magnetic field changes at the centre of the absorber, which is a proposed method for controlling the build-up of canonical angular momentum in a cooling channel. Two AFCs have been produced for MICE and field mapped, however AFC1 achieved a lower maximum operating current ($\approx$ 180 A in isolation) during training than AFC2 ($\approx$ 225 A in isolation). The origin of this difference is not yet understood.

The RFCC module was a series of four RF cavities surrounded by a Coupling Coil (CC), providing re-acceleration between AFC modules. The CC was a large aperture magnet with an inner radius of 725 mm. Winding and training of the CC was completed in 2014, but its integration into a cryostat with the RF cavities, forming the RFCC module, was deemed to be a high-risk schedule item at the August 2014 DOE Review of the MAP Program. At this review a sustainable ionisation cooling demonstration was deemed essential, but the schedule was to be reduced such that it must be completed by the end of the US financial year 2017. Due to the shortened timescale, the CC, and hence RFCC modules, have since been removed from the MICE programme. This necessitates a lattice redesign for a demonstration of ionisation cooling with re-acceleration by 2017.

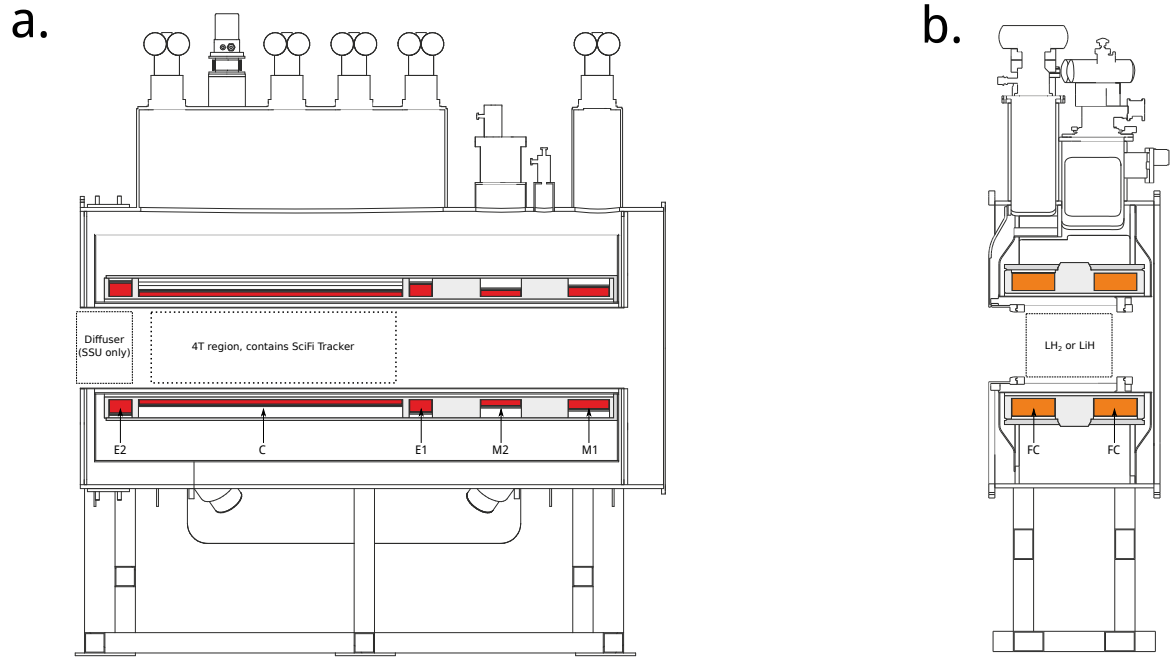


Figure 1: Side-view of (a) a Spectrometer Solenoid, SS, and (b) an Absorber Focus Coil, AFC. The approximate locations of the Diffuser, SciFi tracker and absorbers are indicated by the dashed regions.

Table 2: Proposed absorbers and properties. The equilibrium emittance and fractional change in emittance are quoted for a nominal $(\varepsilon_{\rm in}, \beta_\perp, p_z) = (6, 420, 200)$ beam, and $\frac{dE}{ds}$ is quoted at $p_z = 200\,{\rm MeV}/c$.

| Material | Length (mm) | $X_0$ (mm) | $\frac{dE}{ds}$ (MeV.mm$^{-1}$) | $\varepsilon_{\rm eq}$ ($\pi$ mm.rad) | $\frac{\Delta\varepsilon_N}{\varepsilon_{\rm in}}$ (%) |
|---|---|---|---|---|---|
| $LH_2$ | 350 | 8904 | $-0.031$ | 1.51 | 4.58 |
| LiH | 65 | 971 | $-0.145$ | 2.97 | 2.68 |
| LiH | 32.5 | 971 | $-0.145$ | 2.97 | 1.34 |
| Polyethylene $(CH_2CH_2)_{\rm n}$ | 32.5 | 503.1 | $-0.203$ | 4.09 | 1.17 |

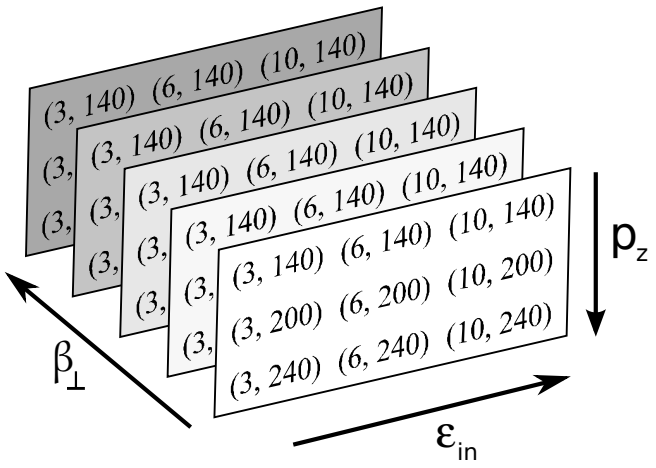


Figure 2: Parameter space that dictates the expected reduction in emittace for an absorber.

## 2.1 Properties that determine cooling performance

A full demonstration of ionisation cooling can be considered in two parts:

- A study of the properties that determine the lattice cooling performance, as dictated by Equation 1
- Demonstration of transverse emittance reduction with longitudinal re-acceleration.

Equation 1 depends on the initial beam emittance, momentum, absorber material and $\beta_\perp$ at the absorber and is studied in MICE Step IV.

The reduction in emittance across a single absorber is measured over a $3 \times 3 \times 5$ $(\varepsilon_{\rm in}, p_z, \beta_\perp)$-grid, as illustrated in Figure 2. By systematically varying these parameters, the equilibrium emittance of the material (Equation 2) is determined. Measurements with the AFC operated in Solenoid and Flip Modes allow for a study of the growth and control of canonical angular momentum.

## 2.2 Sustainable emittance reduction

Once material properties have been fully characterised at Step IV, sustainable ionisation cooling must be demonstrated. This requires restoring the energy lost by the muons passing through the absorber in RF cavities. Hence it depends upon,

- the absorber material,
- the number of absorbers,
- the achievable RF gradient.

MICE Step V used two AFC modules to reduce the transverse emittance, and restored longitudinal momentum in an RFCC module (Figure 3). One RFCC module consisted of four 201 MHz RF cavities, operating at 8 MV/m, surrounded by a Coupling Coil. As there was only one RFCC module, but two absorbers, the beam energy exiting the cooling channel would not be restored to its initial value. This is due to the requirement that the sensitive scintillating fibre tracker modules are protected from X-rays produced by the RF cavities. However, comparisons between measurements with and without the RF powered would demonstrate that sustainable cooling would be possible in a length of cooling channel.

As the RFCC module has been removed from the MICE programme, a new lattice design is necessary to replicate the physics goals of Step V without the CC. Hence, any proposed lattice must,

- observe transverse emittance reduction with re-acceleration,
- observe transverse emittance reduction and longitudinal emittance evolution,

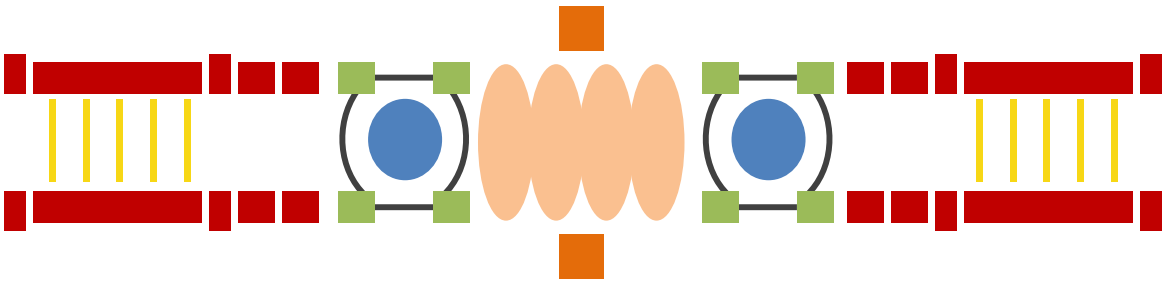

Figure 3: Sketch of the MICE Step V layout: The SS coils are indicated in red, AFC in green, and RFCC in orange. Absorbers are situated in the centres of the AFC modules (blue).

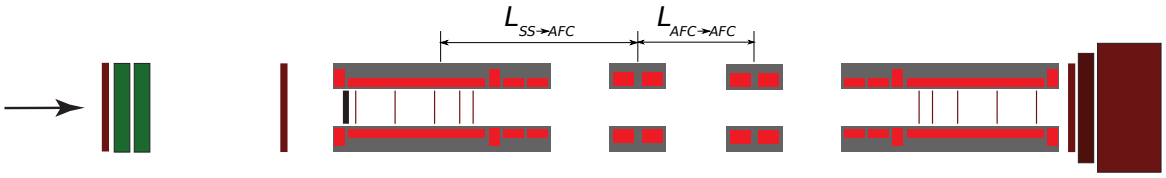


Figure 4: Increasing the separation between the SS and AFC modules improves matching into lattices without an RFCC module. The requirement for an absorber to be within an AFC is also relaxed. $L_{SS\to AFC}$ is the distance between the centre of the SS and AFC modules, and $L_{AFC\to AFC}$ is the distance between the centres of the AFCs.

- observe transverse emittance reduction, longitudinal emittance and angular momentum evolution.

## 3 Lattice design

New lattice designs must use currently fabricated components, and so are restricted to two AFC modules, multiple *single* RF cavities (operating at 10.3 MV/m each) and $LH_2$ or LiH absorbers. A SS can then be placed up- and downstream of the cooling section to measure and match the beam. Figure 4 illustrates this, where the distance between AFC modules, $L_{AFC\to AFC}$, is one key design parameter. The distances between magnets can be expanded or contracted as necessary to contain RF cavities and minimise the value of $\beta_\perp$ at an absorber.

### 3.1 Selected lattice designs

Two lattices have been identified that would fulfil the MICE physics goals, and have been labelled as the *reference* and *alternative* designs. The properties of each design are compared in the following sections. In Figures 6–12, the *reference* lattice is always displayed as a solid, black line, and the *alternative* as a dashed, blue line. The locations of various points of interest (*e.g.* absorber locations) are indicated by vertical lines, labelled in the figure.

The reference and alternative lattices both consist of two single RF cavities, one primary (65 mm) LiH absorber, and two secondary (32.5 mm) LiH secondary ("screening") absorbers. Their differences lie in the separation between the centres of an SS and adjacent AFC, $L_{SS\to AFC}$, AFC to AFC, $L_{AFC\to AFC}$, and the positioning of the RF cavities. Table 3 states these main parameters and Figure 5 shows the positions of the various modules. The reference lattice separates RF cavities and primary absorber by an AFC module, whereas the alternative design places the RF and primary absorber between AFC modules. The role of primary and secondary absorbers is described in Section 3.3.

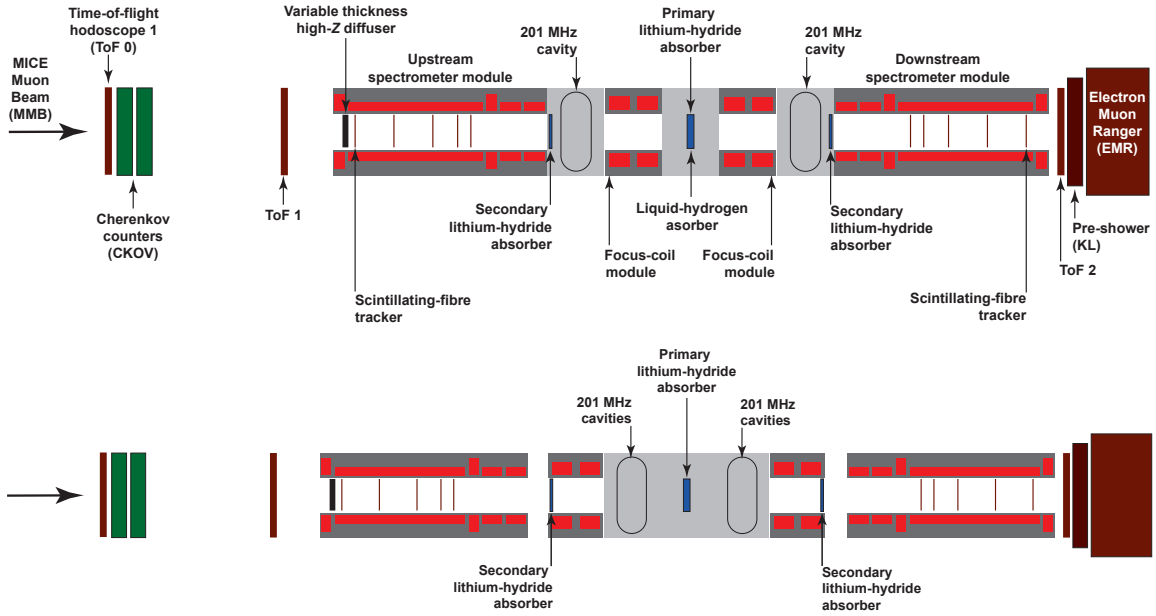


Figure 5: The reference (top) and alternative (bottom) lattice layouts. In both cases, the primary absorber is at the centre of the lattice, and secondary absorbers provide screening between the RF and SS.

Table 3: Design parameters of the reference and alternative lattice designs.

| Parameter | Reference Lattice | Alternative Lattice |
|---|---|---|
| $L_{SS\to AFC}$ (m) | 2.55 | 2.46 |
| $L_{AFC\to AFC}$ (m) | 1.72 | 2.18 |
| RF Gradient (MV/m) | 10.3 | 10.3 |
| No. RF cavities | 2 | 2 |
| No. primary absorbers | 1 | 1 |
| No. secondary absorbers | 2 | 2 |
| $\beta_\perp$ at primary absorber (mm) | 450 | 700 |
| $\beta_\perp$ at secondary absorbers (mm) | 650 | 650 |
| $\beta_{\max}$ at AFC (mm) | 1500 | 1900 |

Table 4: Coil currents used for $(\varepsilon_\perp, p_z) = (6, 200)$ MAUS simulations in the $[++--]$ configuration. Coils are defined in Table 1.

| Coil | Reference Lattice (A) | Alternative Lattice (A) |
|---|---|---|
| Upstream E2 | $+253.00$ | $+255.46$ |
| Upstream C | $+274.00$ | $+288.27$ |
| Upstream E1 | $+234.00$ | $+239.37$ |
| Upstream M2 | $+203.13$ | $+260.83$ |
| Upstream M1 | $+240.61$ | $+230.94$ |
| Upstream AFC1 | $+77.86$ | $+69.81$ |
| Downstream AFC1 | $+77.86$ | $+69.81$ |
| Upstream AFC2 | $-72.94$ | $-67.85$ |
| Downstream AFC2 | $-72.94$ | $-67.85$ |
| Downstream M1 | $-218.39$ | $-210.32$ |
| Downstream M2 | $-187.68$ | $-242.12$ |
| Downstream E1 | $-234.00$ | $-239.37$ |
| Downstream C | $-274.00$ | $-288.27$ |
| Downstream E2 | $-253.00$ | $-255.46$ |

### 3.2 Magnetic field, matching and beam size

The on-axis magnetic field along each lattice is shown in Figure 6. Vertical lines locate the positions of the centre of the AFC modules (red) and the primary absorber (burgundy). The "$[++--]$" configuration shown powers the downstream AFC and SS modules in the opposite sense to the upstream AFC and SS so that the field changes sign at the absorber. This is a desirable feature for studying the cancellation of canonical angular momentum through the lattice. Other possible operating modes are: $[++++]$, where the field does not flip at the absorber, and $[+---+]$, where the field flips *outside* an absorber. All subsequent figures are shown in the favoured $[++--]$ operating mode. Table 4 lists the currents used in this field configuration. For reference, AFC1 achieved a maximum current of $\approx 180$ A in standalone operation in Flip Mode, and 120 A in Solenoid Mode. Hence, both lattice designs operate the AFCs within their current limitations.

In both reference and alternative lattice, the field at the AFC modules is low ($\approx 2$ T) and neither lattice requires that the AFCs be powered at currents higher than that achieved by AFC1. The field at the location of the RF cavities is similar for both lattices ($\approx 1$ T). However, the greater distance between AFC modules in the alternative lattice decreases the field gradient at the absorber with respect to the reference lattice. The magnetic forces acting on the coils have been analysed for both the reference and alternative lattice and were found to be acceptable. In particular, the forces experienced by the AFC modules are below those expected during Step IV.

The transverse betatron function, $\beta_\perp$, is shown in Figure 7 for an initial $(\varepsilon, p_z) = (6, 200)$ beam. The flat region at $z = 4000$ mm corresponds to the flat 4 T field region that contains the SciFi tracker module. The beam is matched from the muon beam line into this region, and then matched (via the M1 and M2 coils) to the lattice cell. Similarly at $z = -4000$ mm, the beam is matched back into the flat 4 T field region from the lattice cell. It is possible to match the beam through both reference and alternative lattice cells, though the reference lattice consistently achieves a smaller $\beta_\perp$ along the channel. Smaller values are preferable. as $\beta_\perp$ influences both emittance reduction (Equation 1) and beam size, .

The physical size of the beam is limited by the apertures of the SS, AFC, and RF windows. Figure 8 shows the radius that contains 95% and 99% of the beam as it passes through the reference (left) and alternative (right)

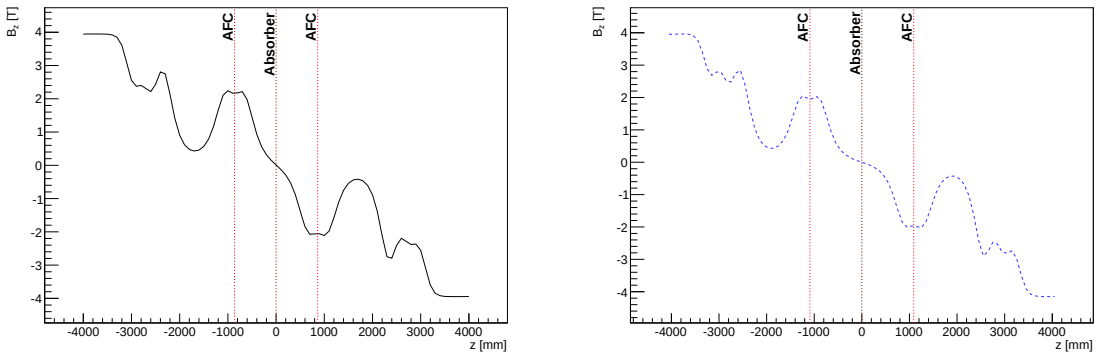


Figure 6: $B_z$ on-axis in $[++--]$ polarity for (left) the reference lattice, and (right) the alternative lattice designs.

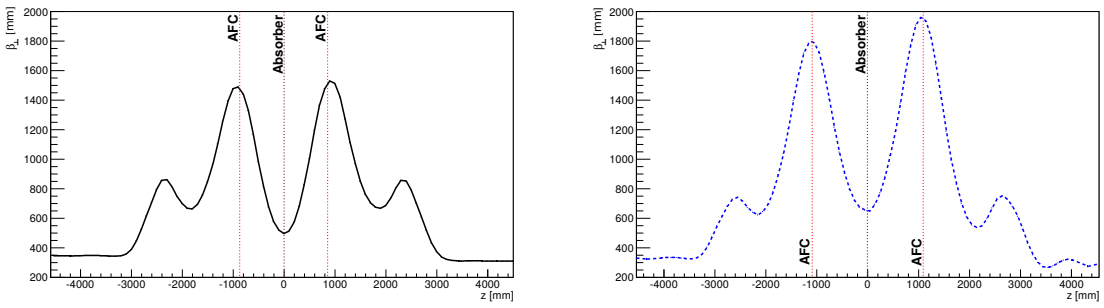


Figure 7: $\beta_\perp$ at 200 MeV/$c$, for (left) the reference lattice, and (light) the alternative lattice designs.

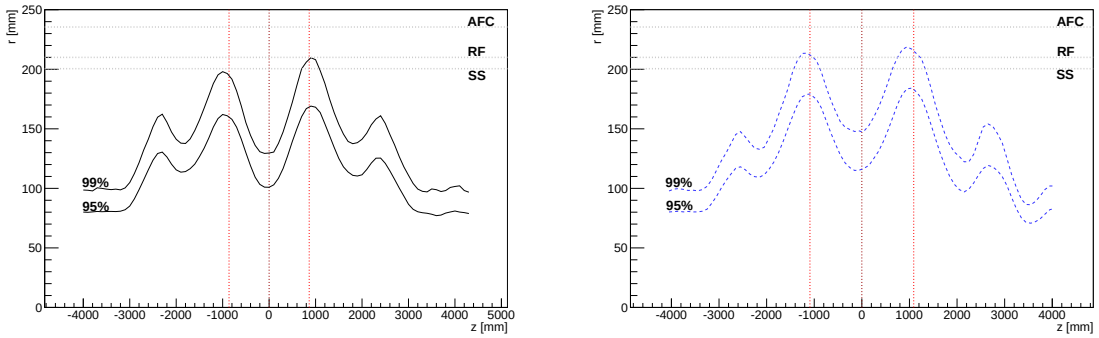


Figure 8: 95 and 99% beam size at $((\varepsilon, p_z) = (6, 200)\,\text{MeV}/c$, for (left) the reference lattice, and (right) the alternative lattice designs. The minimum apertures of the SS, AFC, and RF cavities are indicated by horizontal (dashed) lines.

Table 5: Acceptance criteria for analysis.

| Parameter | Muon accepted |
|---|---|
| Radius at upstream tracker (mm) | $\leq 200.5$ |
| Radius at downstream tracker (mm) | $\leq 200.5$ |
| Charge | $+$ |
| PDG particle ID | $\lvert 13 \rvert$ |

lattices. In both cases, the AFC modules are where the beam is largest and most likely to scrape. However, as the reference lattice has smaller $\beta_\perp$ along the channel, less beam would be scraped compared to the alternative design.

Finally, the transmission of the lattice represents the proportion of muons that remain after scraping and cuts have been accounted for. Table 5 lists the acceptance criteria required by all analyses that follow, which exclude muons that do not appear within the active region of the SciFi trackers and limit particles to positive muons only (as muons may decay).

### 3.3 Absorber placement

The efficiency of a cooling channel is increased by positioning absorbers at locations where $\beta_\perp$ is small. Figure 7 shows that the optimum placement is between the AFC modules. This requirement restricts the absorber material to LiH, which can be positioned in an arbitrary location, specifically outside of an AFC module.

In Step V, the RFCC module was flanked by absorbers that screened the scintillating fibre trackers from X-rays. The Muon Test Area (MTA) has observed that the rate of X-rays from a single MICE RF cavity is not sufficient to damage the SciFi trackers. However, they have yet to be operated in magnetic field and it is still desirable to screen the trackers from the RF cavities. In the both designs, there is a clear line of sight between the RF and trackers. Thus, secondary "screening" absorbers are required to remove the risk of X-ray damage to the trackers. It is estimated that 32.5 mm of LiH (or plastic) would be sufficient for this task. In addition, positioning the secondary absorbers at low $\beta_\perp$ would increase the change in emittance measured across the cell. Therefore, both reference and alternative lattice designs aim to site 32.5 mm of LiH secondary absorber close to the first and third minima in $\beta_\perp$, as shown in Figure 7.

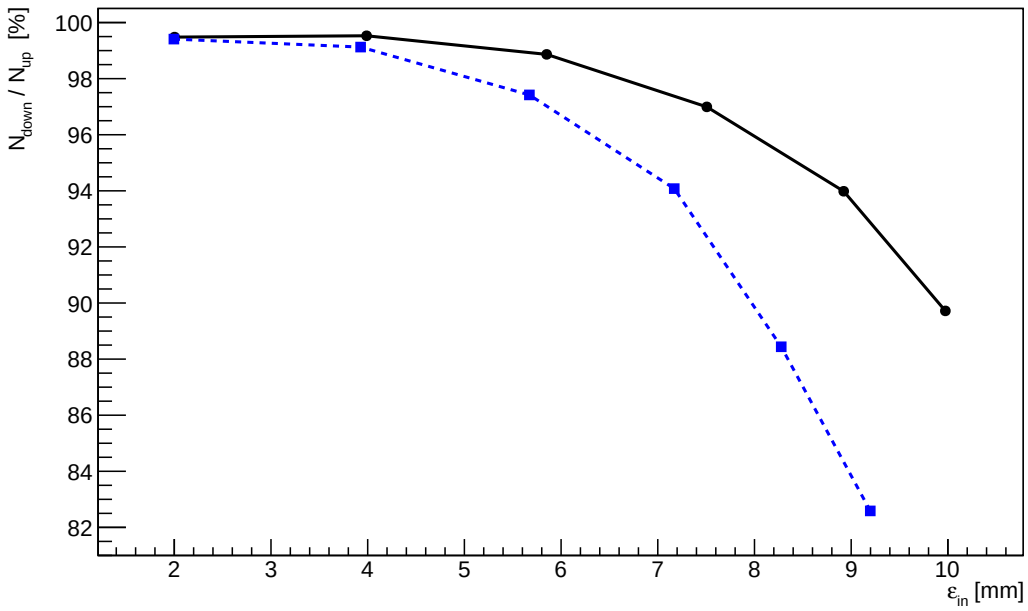


Figure 9: Transmission as a function of initial emittance for (black, solid) the reference lattice, and (blue, dashed) the alternative lattice designs.

### 3.4 Observation of transverse emittance reduction with re-acceleration

Sustainable emittance reduction requires that energy lost in the absorbers is replaced by RF. Both the reference and alternative lattices use two single RF cavities powered at 10.3 MV/m[1] for this purpose, though their positions in the lattice are different. Figure 10 shows the mean beam energy of a $(\varepsilon, p_z) = (6, 200)$ beam as it crosses the lattice. In the reference lattice (left), energy is lost in the upstream tracker and first (secondary) absorber before being partially restored in the first RF cavity ($z \approx -2000$ mm). Further energy is lost in the primary absorber, partially restored in the second RF cavity, and then lost in the final (secondary) absorber. A similar pattern is followed by the alternative lattice, however the first RF cavity is at $z \approx -500$ mm.

A muon passing through two 32.5 mm secondary LiH absorbers and one 65 mm primary LiH absorber would lose $\langle \Delta E \rangle = 18.9$ MeV. Including losses in the SciFi trackers and windows, this increases to 24.3 MeV. The RF gradient achievable in two cavities is insufficient to replace the energy lost in the absorber, therefore a comparison of beam energy with and without RF is required. With RF an energy deficit of $\langle \Delta E \rangle = 19$ MeV would be observed. This measurable difference would confirm that, were more RF cavities or higher RF gradient available, the transverse emittance reduction would be sustainable.

The reduction in transverse emittance, with RF, is shown in Figure 11. The beam is subject to non-linear effects in regions of high $\beta_\perp$, which causes emittance growth in both cases. Nonetheless, a reduction in emittance is observed between the up- and downstream trackers ($z \approx \pm 4000$ mm). The reference lattice achieves a reduction of $\approx 7$ %, and the alternative achieves $\approx 5$ %.

The difference in emittance reduction seen in the reference and alternative lattices is due to the difference in equilibrium emittance (Equation 2) and $\beta_\perp$ at the primary absorber. Figure 12 shows the fractional change in emittance with respect to the input emittance, with an indication the estimated reconstructed measurement error. The reference lattice has a lower equilibrium emittance (shown by the vertical lines in Figure 12), and hence cools larger emittance beams more efficiently.

[1] Including a 10% estimated loss in power due to reflections.

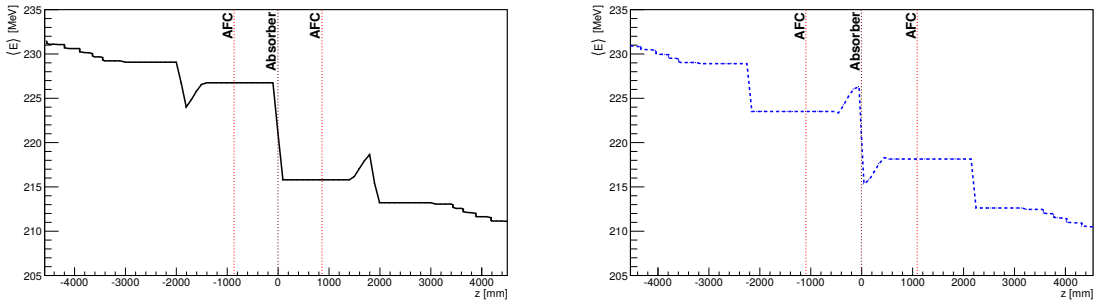


Figure 10: Mean beam energy for (Left) the reference lattice, and (Right) the alternative lattice designs, with re-acceleration.

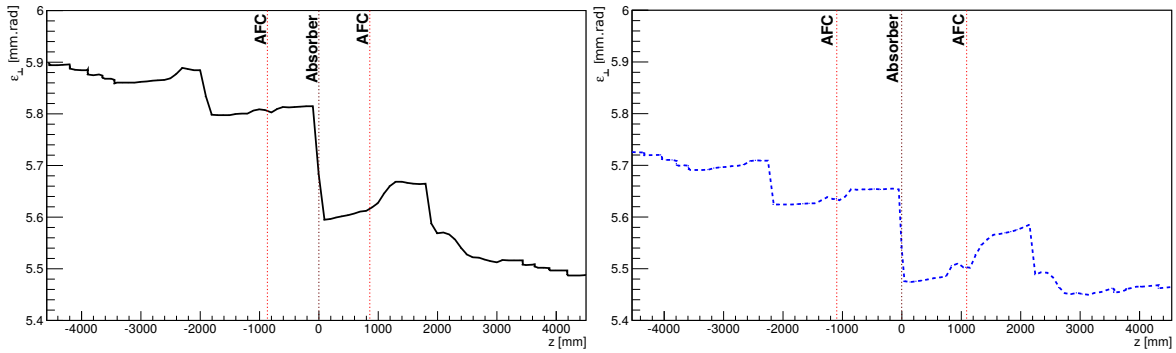


Figure 11: Emittance reduction of a $(\varepsilon, p_z) = (6, 200)$ beam for (left) the reference lattice, and (right) the alternative lattice designs, with re-acceleration.

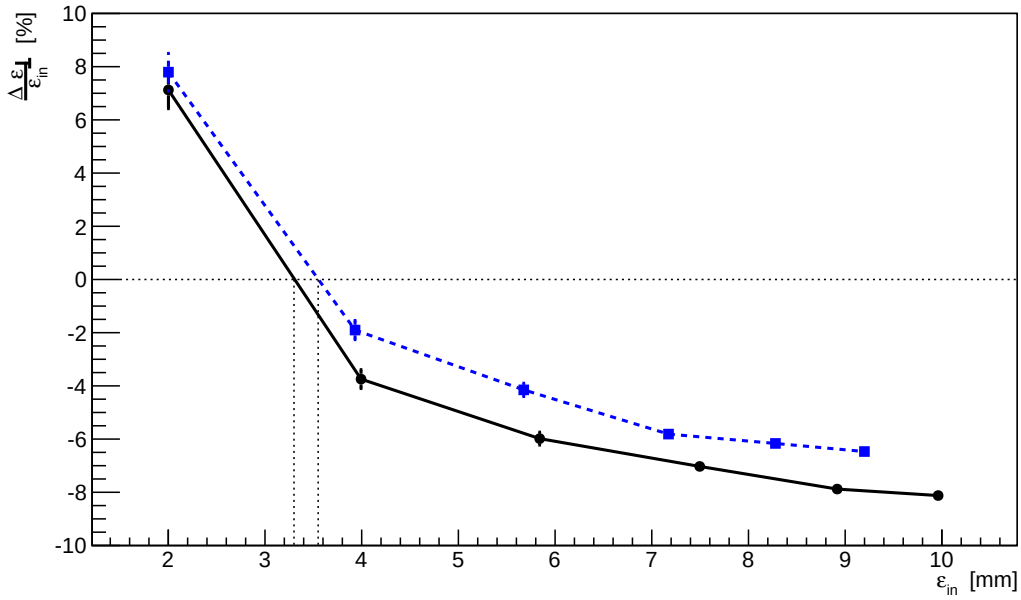


Figure 12: Fractional change in emittance as a function of initial emittance for (black, solid) the reference lattice, and (blue, dashed) the alternative lattice designs, with re-acceleration. The equilibrium emittance for each lattice is indicated by the vertical lines. Error bars estimate the (reconstructed) measurement uncertainty.

Table 6: Critical physics parameters for the MICE Ionisation Cooling Demonstration.

| Parameter | Reference Lattice | Alternative Lattice |
|---|---|---|
| Equilibrium emittance (mm.rad) | 3.30 | 3.55 |
| Minimum transmission (%) | 90 | 82 |
| Observe $\varepsilon_\perp$ reduction | Yes | Yes |
| Demonstrate energy restoration | Yes | Yes |
| Observe evolution of canonical angular momentum | Yes | Yes |
| Observe evolution of $\varepsilon_l$ | Yes | Yes |
| Observe evolution of $\varepsilon_{6D}$ | Yes | Yes |

### 3.5 Observation of longitudinal emittance evolution and 6D cooling

The evolution of longitudinal emittance, $\varepsilon_l$ and 6D emittance, $\varepsilon_{6D}$ is under study. A $\approx 1\,\%$ change in $\varepsilon_{6D}$ has been observed to date. However, both longitudinal and 6D emittance studies depend critically on the degree of momentum spread, energy, time and position correlations introduced into the beam selected in the upstream tracker. Therefore, it is expected that longitudinal emittance can be sustained along the lattice cell as well as a possible reduction in 6D emittance.

## 4 Conclusions

Table 6 gives the performance of the reference and alternative lattice in terms of the MICE physics goals. Both lattices satisfy the physics requirements, however the reference lattice has a lower equilibrium emittance and higher transmission. Therefore the reference lattice best represents the MICE interests[2].

## References


[1] S. Choubey *et al.* International Design Study for the Neutrino Factory, Interim Design Report. 2011.

[2] M. Alsharoa *et al. Phys. Rev. ST Accel. Beams*, 6:081001, Aug 2003.

[3] R. C. Fernow and R. B. Palmer. Solenoidal ionization cooling lattices. *Phys. Rev. ST Accel. Beams*, 10:064001, Jun 2007.

[4] S. Ozaki, R. Palmer, M. Zisman, and J. Gallardo. Feasibility Study-II of a Muon-Based Neutrino Source. Technical report, 2001. BNL-52623.

[5] M. Bogomilov *et al.* The MICE Muon Beam on ISIS and the beam-line instrumentation of the Muon Ionization Cooling Experiment. *Journal of Instrumentation*, 7(5):05009, 2012.

[6] The MICE Collaboration. Characterisation of the muon beams for the Muon Ionisation Cooling Experiment. *European Physical Journal C*, 73(10):2582, 2013.


[2] Pending the outcome of the 6D lattice studies, though the expected differences are, again, small.